24th International Conference on Renewable Energies and Power Quality (ICREPQ'26)
Santander (Spain), 10th to 12th June 2026
ISBN-13: 978-84-09-82044-3

Optimizing MBR Performance: CFD and Experimental Insights on Aeration Design for Fouling Control

S. Khakpour[1], F. Nocera[1], S. Mauro[1], A. Latteri[1], C. Tosto[1], and L. Saitta[1]

[1] Department of Civil Engineering and Architecture (DICAR), University of Catania, via Santa Sofia 64, 95123 Catania (Italy). soroush.khakpour@phd.unict.it, francesco.nocera@unict.it, stefano.mauro@unict.it, alatteri@unict.it, claudio.tosto@unict.it, lorena.saitta@unict.it.

Abstract.

The optimization of membrane bioreactor (MBR) systems is a critical challenge in mitigating membrane fouling. To overcome this issue, a two-phase experimental–computational approach was applied to evaluate the effect of the distance between the aeration pipe and the membrane module on antifouling performance. In the first phase, flat-sheet membranes were fabricated by the NIPS (Non-solvent Induced Phase Separation) method and characterized by field emission scanning electron microscopy (FESEM), pure water flux (PWF), and contact angle measurements. Among the prepared membranes, M2 membrane exhibited the highest PWF of 134 $L \cdot m^{-2} \cdot h^{-1}$, the lowest contact angle of 80.0°, and a more favourable pore size distribution. In the second phase, a computational fluid dynamics (CFD) model was developed to simulate the hydrodynamic conditions around the selected membranes (M2). Increasing the distance improved the uniformity of shear stress distribution across the membrane surfaces. D2 = 60 mm was identified as optimal, as it allowed the system to utilize its full filtration potential while experiencing lower surface friction, thereby reducing fouling. D2 = 60 mm results in the lowest average shear stress (~0.30 Pa), provides the most balanced stress regime, minimizing localized abrasion while maintaining sufficient shear for antifouling, and thereby supporting longer membrane lifespan.

Key words.

Membrane, CFD, MBR, Fouling.

1. Introduction

Membrane bioreactors (MBRs) combine membrane filtration and biological treatment processes to increase treatment efficiency and produce high-quality effluent that may be reused. These systems use submerged membranes to retain biomass and suspended solids, lowering the plant's footprint and sludge production compared to traditional activated sludge systems [1]-[4]. Hydrodynamic variables have a significant impact on the efficiency and performance of membrane bioreactor (MBR) systems since they directly influence membrane fouling and the overall filtration process. Cross-flow velocity, shear stress, and flow regime all influence how successfully pollutants are prevented from collecting on the membrane surface, which is critical for maintaining a high permeate flux while reducing energy consumption. Proper management of these parameters assures proper mixing, improves mass transfer, and extends membrane life, making hydrodynamics an important aspect in the design and operation of MBRs [5]. As a matter of fact, research on hydrodynamic factors and the need to comprehend their impact are becoming more and more intense due to the growing demand for efficient and sustainable wastewater treatment systems. Therefore, improving the operational efficiency of MBR technology requires a thorough grasp of the hydrodynamic performance of MBRs. Hydrodynamic factors play a critical role in MBR performance, helping to minimize operating problems and maximize system efficiency. Flux distribution, shear stress, and mixing intensity are examples of hydrodynamic parameters that have a direct impact on the MBR system's mass transfer mechanisms, membrane fouling, and energy consumption [6],[7]. Computational fluid dynamics (CFD) is a useful tool for predicting fluid behaviour and understanding its impact on hydrodynamics. It helps optimize MBR design and performance by simulating fluid flow, predicting membrane fouling, and analysing treatment processes and scale-up across varied module sizes [8]-[11]. CFD calculations are used to quantify flow field distribution values in MBRs that cannot be detected experimentally. To optimize variables like reactor design, nutrient removal, and energy consumption, it may be possible to obtain trustworthy quantitative results on hydrodynamics performance through the use of CFD. M. Bulgarini et al. numerically investigated the performance of two different lab polymer electrolyte membrane fuel cell configurations, a parallel flow channel configuration and a serpentine flow-field geometry, by using CFD simulation to identify degradation stressors and performance enhancers [12]. Yang et al. used a CFD model to optimize MBR cost-effectively [13]. To forecast gas phase velocities, liquid phase velocities, and membrane surface shear stress values during aeration, Ndinisa et al. employed CFD to model gas–liquid two-phase flow submerged at membrane MBRs [14].

Brannock et al. examined how aeration and membrane configuration, such as the size and placement of baffles, inlets, or membrane orientation, affect the membrane's overall performance [15],[16]. As a result, flow field distribution values in MBRs that cannot be found empirically may be quantified using CFD simulations. Among these parameters, aeration operations receive more attention because of their effect on operation performance and antifouling properties in MBR [17],[18]. Optimizing the distance between the aeration pipe and the membrane module is crucial for boosting energy efficiency, ensuring correct shear stress, enhancing mixing and oxygen transfer, and eliminating dead zones in the system. Proper spacing allows the aeration bubbles to clean the membrane surface effectively without spending too much energy, balancing the need for optimal turbulence to lower energy consumption.

Controlling the shear stress caused by these bubbles helps the system to prevent fouling while also protecting the membrane from damage, extending its life. Furthermore, appropriate spacing allows for better mixing of the combined liquid, resulting in efficient oxygen delivery to microorganisms, which is essential for effective biological treatment processes. Moreover, it helps eliminate dead zones where bubbles may not reach, thus providing consistent aeration and reducing localized fouling. Wang et al. built a novel slug bubbling process through CFD simulation for a large-scale flat sheet MBRs with one hundred membranes; the overall objective was to enhance fouling control through optimization of the bubble distribution and the intensity of the induced shear stress [19]. Wang et al. studied the modified pipe with varied pipe diameters, to optimize the air velocity distribution among all aerators, to achieve the hydrodynamic benefit of shear stress intensification in all areas whilst not using excess air in some partitioning inside the central air supply pipe was studied to have precise control of the air distribution. In addition, the effect of aeration pipe design on velocity distribution and the consequential induced shear stress was paid great attention to enhance the hydrodynamic effect in all channels [20]. Moreover, Wu et al. optimized the membrane unit location and the hydrodynamics of the full-scale membrane bioreactor using CFD [21]. The assumptions and simplifications required for CFD models may result in mistakes. Nevertheless, CFD in MBR systems provides valuable insights into fluid flow patterns, and it also improves membrane cleaning procedures by precisely forecasting shear stress distributions, which helps to prolong membrane life.

Furthermore, it allows the design and scale of MBR systems by simulating various operational scenarios, reducing the need for expensive prototypes and tests. Overall, CFD enhances system performance, reliability, and efficiency by detecting issues [22]. In this study, a three-dimensional CFD simulation was utilized to investigate the effect of the distance between the aeration pipe and membrane module on the fouling phenomenon in the MBR using the commercial software ANSYS FLUENT.

2. Experimental

A. Materials

The primary polymer used to prepare a flat sheet membrane was polyvinyl chloride (PVC; MW 80,000), which was purchased from Sigma Aldrich Co, USA. N,N-dimethylacetamide (DMAc) and polyethylene glycol (PEG; MW = 200 g/mol) were purchased from Merck and Sigma, respectively. The following materials were used: ethanol (99.8%, Sigma), acetone (99%, Merck), and acetic acid (99.85%, Sigma). Synthetic wastewater was used as the feed water for the lab-scale MBR system. Three-dimensional numerical simulation was performed for the different geometries by ANSYS FLUENT software.

B. Membrane Preparation

PVC ultrafiltration membranes were fabricated via the NIPS method. In this method, the total polymer concentration of 17 wt.% was studied, in which different compositions were analysed. PVC and PEG were added to DMAc, and the solution was stirred at 25 °C and 300 rpm for 24 h. Then, the homogeneous dope solution was left still overnight in an oven at 60 °C for degassing. After casting 150 µm membranes and phase inversion at 15 °C, samples were stored in a non-solvent bath (DI water) for the next 24 h in order to complete the phase inversion process. The conditions of the dope solution and bath temperature were studied and optimized for this work [23]. Table I presents the composition of the prepared samples.

Table I. - Membrane composition.

Sample	PVC	PEG	DMAc
M1	17%	0%	83%
M2	17%	3%	80%
M3	17%	5%	78%

C. Characterization of membranes

The contact angle test was applied to find changes in the surface hydrophilicity of membranes using a contact angle goniometer (PGX, Thwing-Albert Instrument Co., USA). Moreover, for calculating the pure water flux (PWF) of synthesized membranes, the sample of membrane was soaked in a water tank that was linked to a vacuum pump so that a trans-membrane pressure of 0.7 bar could be supplied. PWF was calculated by [24]:

$$J_0 = \frac{\boldsymbol{V}}{\boldsymbol{At}} \quad (1)$$

where J_0 is the penetration flow of membrane for unadulterated water flux (l m^{-2} h^{-1}), V is compact volume of water (l), A is the membrane's efficient surface area (m^2), and t is time (h). Performance of the prepared membranes was also measured by activated sludge for 250 minutes with the following conditions in Table II.

Table II. - The operation conditions for the MBR test system.

Parameters	Values
MLSS (Mixed Liquor Suspended Solid) (g/L)	6 - 7
Sludge retention time (SRT) (day)	30
Hydraulic retention time (HRT) (h)	37
Chemical oxygen demand (COD) (g/L)	3
Aeration (m/s)	2

Furthermore, the morphology of the produced membranes was visualized using a Field Emission Scanning Microscope (FESEM; MIRA3 FEG-SEM, Tescan).

3. CFD modelling

D. Model geometry

A lab-scale MBR was designed and produced (Fig. 1 and Fig. 2). However, the dimensions of the calculation area were based on the real size of the lab-scale flat sheet MBR (L × W × H = 180 mm × 180 mm × 335 mm). Five membrane modules (L × W × H = 160 mm × 2 mm × 200 mm) were installed in the reactor. To reduce sludge inflow, three aeration pipes (L × d = 160 mm × 10 mm) were located at 60 mm below the membranes, and 13 aeration holes (2 mm in diameter) were inclined 90° downward and distributed on both sides of each aeration pipe. The experiment utilized a flat sheet ultrafiltration PVC membrane with an optimized pore size of 0.3 µm (the purpose of choosing this value will be discussed further). The schematic diagram of the MBR was employed in the CFD model, and the dimension values listed in Table III.

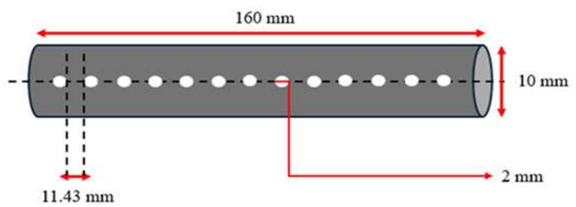

Fig. 1. Schematic diagram of the aeration pipe parameters.

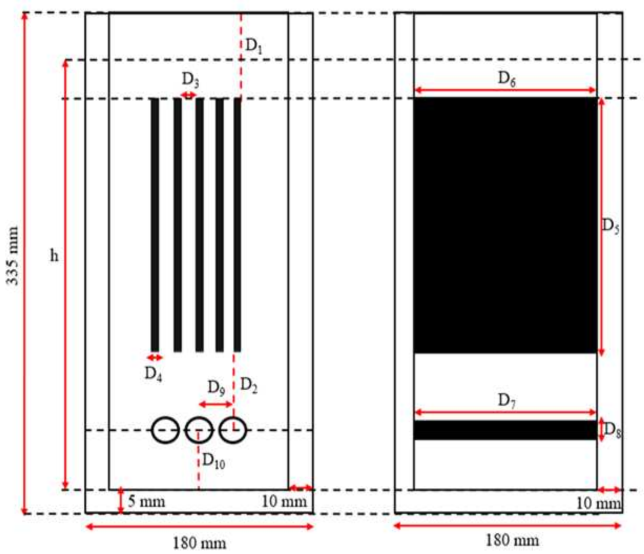

Fig. 2. Schematic of the MBR system

Table III. - Symbols and initial values of dimensions for MBR design.

Symbol	Parameter	Value
D1	The distance from the membrane module top to tank surface	60 mm
D2	The distance between membranes and aeration pipe center	60 mm
D3	The distance between membranes	8 mm
D4	The membrane width	2 mm
D5	The membrane Height	200 mm
D6	The membrane Length	160 mm
D7	The aeration pipe Length	160 mm
D8	The aeration pipe diameter	10 mm
D9	The distance of aeration pipes (center to center)	20 mm
D10	The distance from the center of aeration pipes to the bottom of tank	10 mm
h	The effective height (height of liquid in the tank)	300 mm

The gas–liquid flow was modelled using the Euler–Euler multiphase approach, with turbulence described by the RNG k–ε model. The SIMPLE algorithm was used for pressure–velocity coupling, and second-order upwind schemes were applied. Convergence was reached at residuals below 10^{-4} . A mesh-independence check up to 475,959 cells showed variations in wall shear stress below 3%, confirming adequate mesh resolution.

4. Results and Discussion

E. Membrane characterization

The hydrophilicity of the prepared membranes was evaluated using contact angle measurements. As shown in Fig. 3, the addition of PEG reduced the contact angle, indicating increased hydrophilicity. The neat PVC membrane (M1) showed the highest contact angle of 91.8°, while M2 and M3 decreased to 80.0° and 82.3°, respectively, due to PEG and the formation of more surface pores. The PEG incorporation not only lowered the contact angle but also improved pure water flux (PWF). The oxygen-containing functional groups in PEG enhanced membrane hydrophilicity, with M2 and M3 outperforming M1. Uniform nanocomposite distribution further increased PWF, rising from 82 $L\cdot m^{-2}\cdot h^{-1}$ for M1 to 134 $L\cdot m^{-2}\cdot h^{-1}$ for M2.

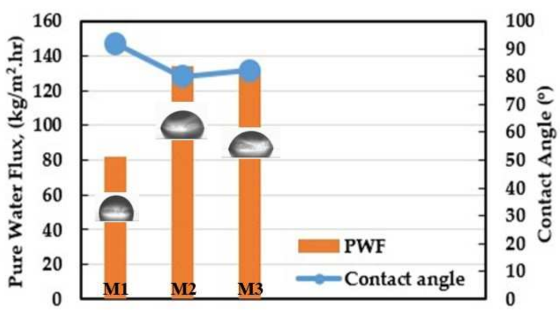

Fig. 3. Pure water flux and contact angle measurement and comparison.

The surface and cross-sectional FESEM images of the prepared membranes are shown in Fig. 4. It can be seen the increasing of pores in membranes has affected the structure. The pure PVC membrane surface has less pores in comparison with M2 and M3 membranes. Larger holes could be detected as the concentration of PEG polymer was raised from 0 to 5 wt.%. PEG polymer was seen to act like a hydrophilic stabilizer that influenced the speed of exchange between solvent and non-solvent during phase division. This eventually triggered the creation of bigger hole channels.

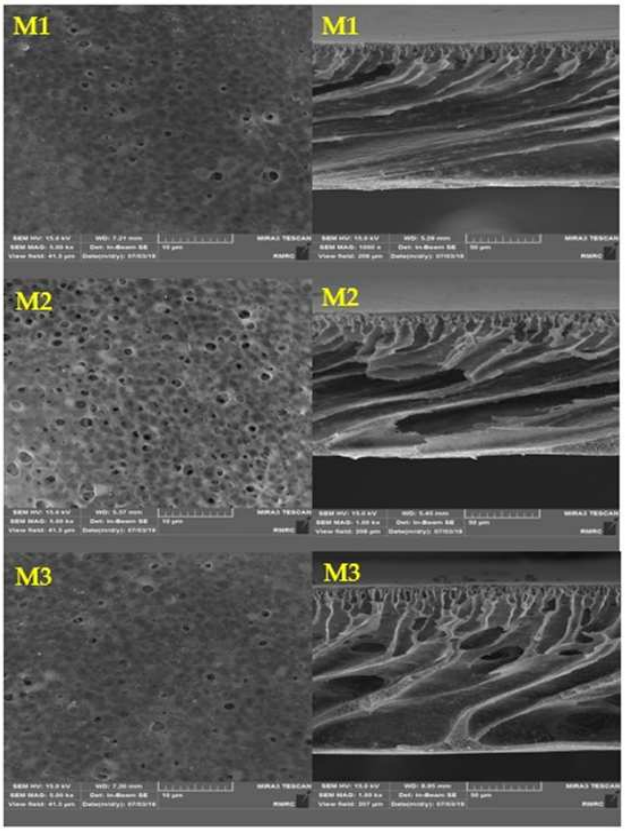

Fig. 4. Surface (left) and cross-section (right) FESEM images of prepared membranes.

Based on the characterization results, M2 demonstrated the most favorable combination of properties among the three membranes. It exhibited the highest pure water flux (134 $L\cdot m^{-2}\cdot h^{-1}$) and the lowest contact angle (80.0°), indicating superior hydrophilicity compared to M1 and M3. FESEM analysis further confirmed that M2 possessed an optimal pore structure, with well-distributed and adequately sized surface pores that facilitate water penetration. Therefore, considering the combined results of PWF, contact angle, and FESEM analyses, M2 was selected as the best-performing membrane and used in the subsequent CFD simulations to evaluate hydrodynamic behavior and antifouling performance in the MBR system.

F. MBR filtration

Fig. 5 showed the performance of the membranes during the MBR process. All purification tests were organized at a sub-critical pressure of 0.1 bar and processed until the flow reached a fixed amount. Initially, evaluations were conducted on the flow of unadulterated water for 90 minutes, and then purification of MBR was carried out for another 250 min. All samples were tested in the same condition and with the same distance of D2 = 60 mm from aeration pipes in order to find the best sample for further characterizations. It can be seen that the flux value of M2 membrane was decreased from 60 $l.m^{-2}.h^{-1}$ to about 48 $l.m^{-2}.h^{-1}$. Initial and final fluxes of M2 membrane are higher than those of M1 and M3 membranes.

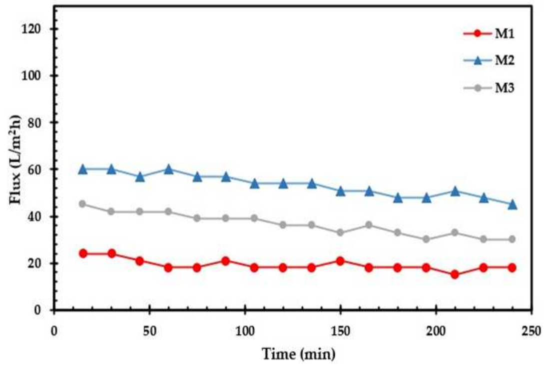

Fig. 5. Flux-time behavior of prepared membranes in MBR.

The flux of M2 membrane was higher than that of the neat PVC membrane. Thus, membrane hydrophilicity has shown its effectiveness in improving activated sludge filtration flux. Moreover, the slope of the flux decline of the M3 membrane is sharper than other membranes at the beginning of the filtration. It can be attributed to the much lower surface pores of this membrane, which leads to less filtration and high fouling. However, after a 250-minute filtration process, the final flux of the M2 membrane is still higher than other membranes, which is due to the presence of an optimized amount of hydrophilic PEG in the membrane.

G. CFD analysis results

According to Fig. 6, at the largest distance of D2 = 60 mm between the aeration pipes and the membranes, air bubbles have more space to spread and rise before interacting with the membrane surfaces. This increased space enables a more uniform distribution of bubbles, thereby enhancing the scouring effect and reducing fouling. The fluid dynamics analysis revealed a more even velocity contour and reduced turbulence near the membranes. The lower friction forces on the membranes prevent excessive biofilm buildup, resulting in longer membrane lifespan and reduced maintenance costs. Additionally, this setup is more energy-efficient, as it requires less power to maintain effective fluid movement and aeration. According to the movement path of the air bubble, reducing the distance to D2 = 50 mm changes the behaviour of the air bubbles, causing them to become more concentrated, which leads to more frequent collisions and the formation of larger bubbles, which might rise more quickly. The closer proximity increases fluid velocities and turbulence near the membranes, which may enhance cleaning in certain areas but also increase the risk of uneven fouling and membrane wear. Furthermore, Fig. 7 represented the effect of changing D2 on the surface friction contour and wall shear stress. Increasing D2 to 60 mm leads to a gradual decrease in shear stress on the membrane surface. This effect can be attributed to the role of D2 in regulating the area through which the external fluid enters the membrane modules. When the distance is reduced to 50 mm, the surface friction in the vicinity of the membrane surfaces increases. Consequently, this elevated friction may accelerate membrane wear, thereby increasing the susceptibility of the membranes to damage and fouling.

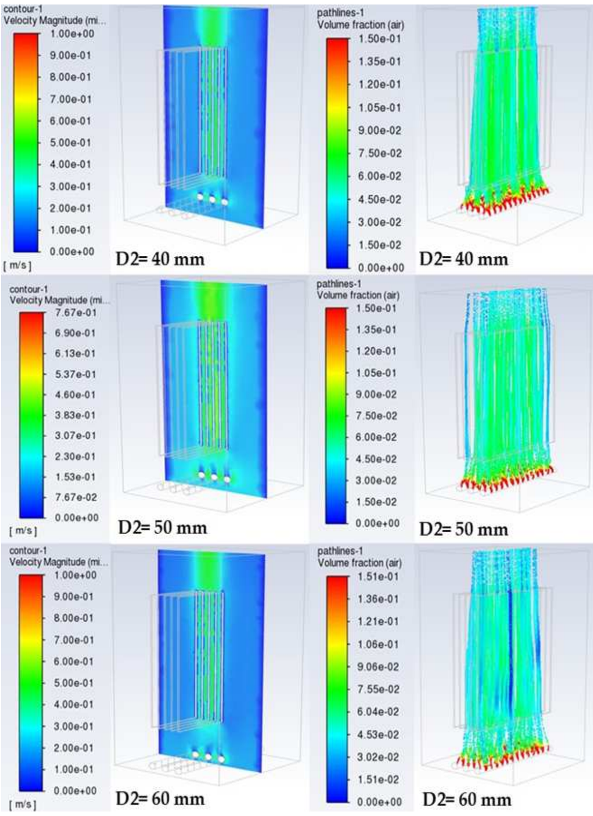

Fig. 6. The effect of changing D2 on the movement path of the air bubble (right), and fluid velocity contour (left).

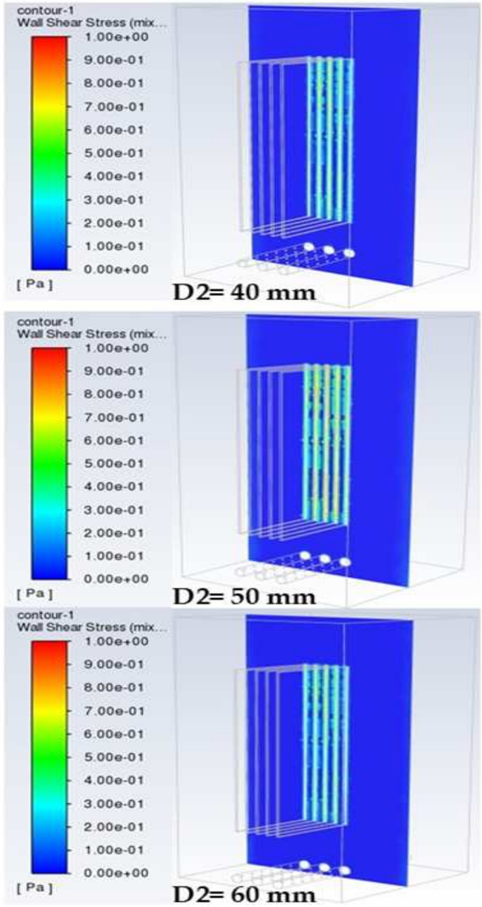

Fig. 7. The effect of changing D2 on the surface friction contour and wall shear stress.

At a spacing of 40 mm, the system exhibits the highest degree of surface friction, which generates a markedly uneven aeration pattern within the membrane modules. In contrast, a spacing of 60 mm represents the most energy-efficient configuration. At this distance, the flow remains well balanced, resulting in reduced frictional resistance and lower power demands to sustain effective aeration and fluid movement. A spacing of 50 mm yields intermediate performance but is still less energy-efficient than the 60 mm configuration. The elevated turbulence and friction at this distance necessitate additional energy input to preserve adequate aeration and fluid dynamics, increasing operating expenses.

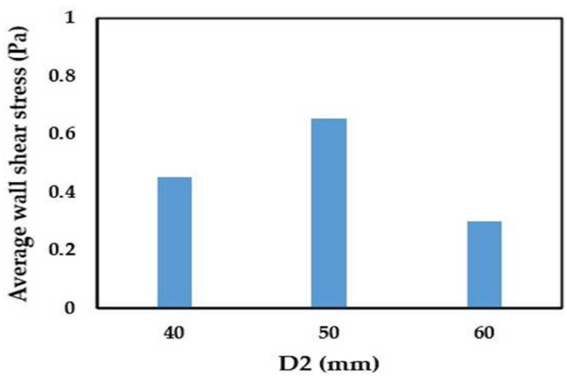

Fig. 8. The effect of the distance between aeration pipes and membranes (D2) on wall shear stress (overall view).

Fig. 8. quantifies how the aeration–membrane spacing (D2) influences the average wall shear stress on the membrane surfaces. At D2 = 40 mm, the average shear stress is approximately 0.45 Pa, indicating strong bubble–membrane interactions caused by the reduced spacing. This value reflects the intensified turbulence and concentrated bubble impacts that occur when air has limited vertical space to disperse before reaching the membranes. Increasing the spacing to D2 = 50 mm produces the highest average shear stress (~0.65 Pa). However, this elevated shear is less uniformly distributed and may contribute to uneven scouring and accelerated mechanical wear. In contrast, D2 = 60 mm results in the lowest average shear stress (~0.30 Pa).

Although higher shear stress can enhance membrane scouring in MBR systems, excessively high or localized shear may also accelerate membrane surface abrasion and cause uneven fouling due to concentrated bubble collisions. In this study, the 60 mm spacing provides a more uniform hydrodynamic regime where the shear stress (~0.30 Pa) remains sufficient for fouling mitigation while reducing mechanical stress on the membrane surface, resulting in a more stable and energy-efficient operation.

At this spacing, bubbles rise through a larger open volume, enabling broader dispersion and reducing direct collisions with the membrane surface. The lower and more uniform shear reflects a more stable hydrodynamic condition where fouling is effectively mitigated without imposing excessive mechanical stress. Overall, the results demonstrate that although both 40 mm and 50 mm generate higher shear, D2 = 60 mm provides the most balanced stress regime, minimizing localized abrasion while maintaining sufficient shear for antifouling, and thereby supporting longer membrane lifespan and improved operational stability.

5. Conclusion

Among the fabricated membranes, the PVC-based M2 membrane exhibited higher permeability, hydrophilicity, and pore structure, confirming its suitability for enhanced filtration efficiency and reduced fouling. CFD simulations further revealed that an aeration pipe–membrane spacing of 60 mm provides the most favourable hydrodynamic conditions, yielding uniform bubble distribution, balanced shear stress, and lower surface friction, leading to improved antifouling performance, extended membrane lifespan, and reduced energy consumption. D2 = 60 mm results in the lowest average shear stress (~0.30 Pa), provides the most balanced stress regime, minimizing localized abrasion while maintaining sufficient shear for antifouling, and thereby supporting longer membrane lifespan. Despite these benefits, the study is limited by the laboratory scale of the MBR and the assumptions inherent complexity of full-scale operational environments. Future work should validate these findings under real wastewater conditions and explore how variable loading, long-term operation, and module scaling influence hydrodynamics and fouling behaviour. Overall, the combined experimental–computational approach presented here offers a practical pathway for optimizing membrane design and aeration configuration in MBR systems.

References

[1] P. Krzeminski, L. Leverette, S. Malamis and E. Katsou, “Membrane bioreactors – a review on recent developments in energy reduction, fouling control, novel configurations, LCA and market prospects”, Journal of Membrane Science (2017). Vol. 527, pp. 207-227.

[2] F. Meng, S. Zhang, Y. Oh, Z. Zhou, H. S. Shin and S. R. Chae, “Fouling in membrane bioreactors: an updated review”, Water Research (2017). Vol. 114, pp. 151-180.

[3] M. Wu, Y. Chen, H. Lin, L. Zhao, L. Shen, R. Li, Y. Xu, H. Hong and Y. He, “Membrane fouling caused by biological foams in a submerged membrane bioreactor: mechanism insights”, Water Research (2020). Vol. 181, 115932.

[4] M. Wu, M. Zhang, L. Shen, X. Wang, D. Ying, H. Lin, R. Li, Y. Xu and H. Hong, “High propensity of membrane fouling and the underlying mechanisms in a membrane bioreactor during occurrence of sludge bulking”, Water Research (2023). Vol. 229, 119456.

[5] M. Yang, D. Yu, M. Liu, L. Zheng, X. Zheng, Y. Wei, F. Wang and Y. Fan, “Optimization of MBR hydrodynamics for cake layer fouling control through CFD simulation and RSM design”, Bioresource Technology (2017). Vol. 227, pp. 102-111.

[6] T. J. Rector, J. L. Garland and S. O. Starr, “Dispersion characteristics of a rotating hollow fiber membrane bioreactor: effects of module packing density and rotational frequency”, Journal of Membrane Science (2006). Vol. 278, pp. 144-150.

[7] K. Xiao, S. Liang, X. Wang, C. Chen and X. Huang, “Current state and challenges of full-scale membrane bioreactor applications: a critical review”, Bioresource Technology (2019). Vol. 271, pp. 473-481.

[8] R. W. Samstag, J. J. Ducoste, A. Griborio, I. Nopens, D. J. Batstone, J. D. Wicks, S. Saunders, E. A. Wicklein, G. Kenny and J. Laurent, “CFD for wastewater treatment: an overview”, Water Science Technology (2016). Vol. 74, pp. 549-563.

[9] X. Guo, Y. Wang, H. Zhang, P. Li and C. Ma, “Numerical and experimental investigation for cleaning process of submerged outside-in hollow fiber membrane”, Water Science Technology (2017). Vol. 76, pp. 1283-1299.

[10] Y. Shi, Z. Wang, X. Du, B. Gong, V. Jegatheesan and I. U. Haq, “Recent advances in the prediction of fouling in membrane bioreactors”, Membranes (2021). Vol. 11, 381.

[11] S. J. Poormohamadian, H. Koolivand, M. Koolivand-Salooki and M. Esfandyari, “Numerical modeling of wastewater treatment using hollow fiber membrane contactors based on the stiff spring method”, South African Journal of Chemical Engineering (2022). Vol. 40, pp. 21-31.

[12] M. Bulgarini, A. Della Torre and A. Baricci, “Computational Fluid Dynamic Investigation of Local Flow-Field Conditions in Lab Polymer Electrolyte Membrane Fuel Cells to Identify Degradation Stressors and Performance Enhancers”, Energies (2024). Vol. 17, 3643.

[13] M. Yang, Y. Wei, X. Zheng, F. Wang, X. Yuan, J. Liu, N. Luo, R. Xu, D. Yu and Y. Fan, “Hydraulic optimization of membrane bioreactor via baffle modification using computational fluid dynamics”, Bioresource Technology (2014). Vol. 175, pp. 633-637.

[14] N. V. Ndinisa, A. G. Fane, D. E. Wiley, D. F. Fletcher, “Fouling Control in a Submerged Flat Sheet Membrane System: Part II—Two□Phase Flow Characterization and CFD Simulations”, Separation Science and Technology (2006). Vol. 41, pp. 1411-1445.

[15] M. Brannock, Y. Wang and G. Leslie, "Mixing characterisation of full-scale membrane bioreactors: CFD modelling with experimental validation", Water Research (2010). Vol. 44, pp. 3181-3191.
[16] M. Brannock, G. Leslie, Y. Wang and S. Buetehorn, "Optimising mixing and nutrient removal in membrane bioreactors: CFD modelling and experimental validation", Desalination (2010). Vol. 250, pp. 815-818.
[17] S. M. Mohan, S. Nagalakshmi, "A review on aerobic self-forming dynamic membrane bioreactor: formation, performance, fouling and cleaning", Journal of Water Process Engineering (2020). Vol. 37, 101541.
[18] S. Zhang, K. Yang, W. Liu, Y. Xu, S. Hei, J. Zhang, C. Chen, X. Zhu, P. Liang, X. Zhang, X. Huang, "Understanding the mechanism of membrane fouling suppression in electro-anaerobic membrane bioreactor", Chemical Engineering Journal (2021). Vol. 418, 129384.
[19] B. Wang, K. S. Zhang and R. W. Field, "Novel aeration of a large-scale flat sheet MBR: a CFD and experimental investigation", AIChE Journal (2018). Vol. 64, pp. 2721-2736.
[20] B. Wang, Y. Zhang, Y. Fang, K. Zhang and R. W. Field, "Aeration pipe design for free bubbling hydrodynamic optimization of flat sheet MBRs", Journal of Membrane Science (2022). Vol. 646, 120222.
[21] Q. Wu, X. Yan, K. Xiao, J. Guan, T. Li, P. Liang and X. Huang, "Optimization of membrane unit location in a full-scale membrane bioreactor using computational fluid dynamics", Bioresource Technology (2018). Vol. 249, pp. 402-409.
[22] F. Cortés-Juan, B. Balannec and T. Renouard, "CFD-assisted design improvement of a bench-scale nanofiltration cell", Separation and Purification Technology (2011). Vol. 82, pp. 177-184.
[23] S. Khakpour, Y. Jafarzadeh and R. Yegani, "Incorporation of graphene oxide/nanodiamond nanocomposite into PVC ultrafiltration membranes", Chemical Engineering Research and Design (2019). Vol. 150, pp. 60-70.
[24] M. Sayadi, S. Khakpour, Y. Jafarzadeh, "Effects of PMMA-PEG Copolymer on the Structure and Performance of PVC Membranes for Oily Wastewater Treatment", International Journal of Chemical Engineering (2025). 8183253.